

Did the Universe Reionize at Redshift Six?

Rennan Barkana

Canadian Institute for Theoretical Astrophysics, 60 St. George Street, Toronto, Ontario, M5S 3H8, CANADA;

Present address: *School of Physics and Astronomy, Tel Aviv University, Tel Aviv 69978, ISRAEL*

barkana@wise.tau.ac.il

ABSTRACT

In light of recent observations of spectra of the quasars SDSS 1030+0524 (Becker et al. 2001) and SDSS 1044-0125 (Djorgovski et al. 2001), we study the observational signatures of different stages of the reionization epoch. During the initial, pre-overlap stage, the hydrogen throughout the universe is neutral except for isolated H II bubbles due to individual ionizing sources. The central stage of reionization is the overlap stage, during which the individual H II bubbles overlap each other and reionize the low-density gas which takes up most of the volume of the universe. Some neutral hydrogen remains in dense clumps which are then slowly reionized during post-overlap. We show that both of the recent observations are consistent with the post-overlap stage. Becker et al. (2001) may have observed the universe in the era before the end of overlap, but a conclusive proof of this requires the observation of similar intervals of Gunn-Peterson absorption at the same redshift along several additional lines of sight.

Key Words: galaxies: high-redshift, cosmology: theory, galaxies: formation

PACS: 98.80.-k, 98.65.Dx, 98.62.Ai

1. Introduction

Until recently, the highest redshift detected for a quasar was $z = 5.8$ (Fan et al. 2000). Although the spectrum showed strong absorption short-ward of the Lyman- α line of the quasar, the detection of transmitted flux in this spectrum was taken to imply that reionization was complete by $z \sim 6$, since even a small neutral fraction in the IGM would have produced total absorption, a fact first pointed out by Gunn & Peterson (1965). The most natural explanation for reionization is photo-ionizing radiation produced by an early generation of stars and quasars; recent calculations of structure formation in cold dark matter (CDM) models find that reionization should naturally occur at $z \sim 6-12$ (Haiman & Loeb 1997, 1998; Gnedin & Ostriker 1997; Chiu & Ostriker 2000; Gnedin 2000, and for comprehensive reviews on the subject of reionization and the first galaxies, see Barkana & Loeb 2001; Loeb & Barkana 2001).

The reionization of hydrogen is expected to involve several distinct stages. The initial, “pre-overlap” stage (using the terminology of Gnedin 2000) consists of individual ionizing sources turning on and ionizing their surroundings. The radiation from the first galaxies must make its way through the surrounding gas inside the host halo, then through the high-density region which typically surrounds each halo. Once they emerge, the ionization fronts propagate more easily into the low-density voids, leaving behind pockets of neutral, high-density gas. During this period the IGM is a two-phase medium characterized by highly-ionized regions separated from neutral regions by sharp ionization fronts. The central, relatively rapid “overlap” phase of reionization begins when neighboring H II regions start to overlap. Whenever two ionized bubbles are joined, each point inside their common boundary becomes exposed to ionizing photons from both sources. Therefore, the ionizing intensity inside H II regions rises rapidly, allowing those regions to expand into high-density gas. This process leads to a state in which the low-density IGM is highly ionized and ionizing radiation reaches everywhere except for gas located inside self-shielded, high-density clouds. Some neutral gas does, therefore, remain in high-density structures which correspond to Lyman Limit systems and damped Ly α systems seen in absorption at lower redshifts. The ionizing intensity continues to grow during this “post-overlap” phase, as an increasing number of ionizing sources becomes visible to every point in the IGM.

Recently, Djorgovski et al. (2001) and Becker et al. (2001) found, for the first time, broad regions of Gunn-Peterson absorption in quasar spectra, with high optical depth throughout each region. Djorgovski et al. (2001) observed the quasar discovered by Fan et al. (2000) with a higher spectral resolution and high signal to noise, and discovered a dark region which is ~ 5 Mpc long at $z \sim 5.3$. Becker et al. (2001) discovered the most distant source of light observed to date, a quasar at $z = 6.28$; the spectrum showed a dark region of ~ 15 Mpc length extending right up to $z = 6.15$, where the emission of the quasar itself may begin to have an effect. Since even a small neutral fraction in the IGM can produce these long stretches of strong absorption, it has thus far been unclear whether these observations indeed herald the empirical discovery of the overlap era; instead, these observations may only be approaching the end of overlap, which itself occurred at an even higher redshift than that probed by current observations.

In this paper, we construct a model of the statistics of neutral and ionized regions during reionization, in order to interpret the recent observations. Our goal is to use the observations to infer the state of the IGM at $z \sim 6$, and specifically to determine whether the universe has indeed been observed during or even before the overlap stage. We focus on the observable property which is not found at low redshifts but is a new feature of the recent observations, namely long intervals of continuous strong Ly α absorption. The model must be statistical, since the ionizing intensity in the IGM is extremely inhomogeneous during reionization and for some period afterwards. Given the small sample of lines of sight probed thus far, we seek to address the question of whether a statistical fluctuation could produce the observed Gunn-Peterson absorption even if the entire IGM has already been reionized at the observed redshift. Since the properties of ionizing sources at these high redshifts are speculative at present, having almost no observational constraints, we strive to

obtain model-independent conclusions. We present our model in §2 and the results in §3. We then confront the model results with the observations in §4. Finally, we give our conclusions in §5.

The basic theoretical framework in which the matter content of the universe is dominated by CDM has recently received a major confirmation from measurements of the cosmic microwave background (Netterfield et al. 2001; Lee et al. 2001; Halverson et al. 2001). Based primarily on these measurements, in this paper we use cosmological parameters $\Omega_m = 0.35$, $\Omega_\Lambda = 0.65$, $\Omega_b = 0.05$, $\sigma_8 = 0.85$, $n = 1$, and $h = 0.65$, where Ω_m , Ω_Λ , and Ω_b are the total matter, vacuum, and baryon densities in units of the critical density, σ_8 is the root-mean-square amplitude of mass fluctuations in spheres of radius $8 h^{-1}$ Mpc, and $n = 1$ corresponds to a primordial scale-invariant power spectrum.

2. Modeling the Statistics of Gunn-Peterson absorption

2.1. Ionizing Sources

In this section we describe a model which allows us to predict the observable properties of quasar spectra during the various stages of reionization. Roughly speaking, the question we wish to address is the following; if we consider spectra taken along random lines of sight through the universe, at a given redshift, then what fraction of these spectra will be similar to those that have actually been observed? We define the similarity of spectra in terms of the presence or absence of long intervals of strong Ly α absorption. The absorption depends on the distribution of gas density in the IGM and on the ionization state of the gas, which in turn depends on the properties of ionizing sources. Our strategy is to construct a model which is general enough to include a wide range of possible scenarios, given the current paucity of direct observational constraints on, for example, the properties of the ionizing sources. While we study the dependence of the results on the various input parameters, we especially seek a model-independent probe of the reionization state of the IGM. In this subsection we describe our model for the properties of ionizing sources; in §2.2 we model the gas density and ionization state, and obtain its opacity; finally, in §2.3 we discuss the physical quantities that we calculate in order to compare our model with the observations.

Galaxies and the ionizing sources within them form in halos in which gas can accumulate and cool. At high redshift, gas can cool efficiently in halos down to a virial temperature of $\sim 10^4$ K or a circular velocity of $V_c \sim 16.5 \text{ km s}^{-1}$ with atomic cooling. Cooling is possible down to $V_c \sim 2 \text{ km s}^{-1}$ with molecular hydrogen (H_2) cooling, but molecular hydrogen is fragile and is expected to be photo-dissociated well before reionization unless mini-quasars¹ make a large contribution to the ionizing intensity (Haiman et al. 1997, 2000). Before reionization, the IGM is cold and neutral, and these cooling requirements set the minimum mass for halos which can host galaxies. During reionization,

¹A mini-quasar is an accreting central black hole in a dwarf galaxy.

however, when a volume of the IGM is ionized by stars, the gas is heated to a temperature $T_{\text{IGM}} \sim 1-2 \times 10^4$ K. We adopt a standard temperature of $T_{\text{IGM}} = 1.5 \times 10^4$ K, and then the linear Jeans mass corresponds to a virialized halo with a circular velocity of

$$V_J = 82 \left(\frac{T_{\text{IGM}}}{1.5 \times 10^4 \text{K}} \right)^{1/2} \text{ km s}^{-1}, \quad (1)$$

where this value is essentially independent of redshift. Even halos well below the Jeans mass can pull in some gas once the dark matter collapses to the virial overdensity. For simplicity, we adopt a sharp cutoff associated with this suppression, at a circular velocity of $V_c = V_J/2$, based on the results of numerical simulations (Thoul & Weinberg 1996; Quinn et al. 1996; Weinberg et al. 1997; Navarro & Steinmetz 1997; Kitayama & Ikeuchi 2000). However, this pressure suppression is not expected to cause an immediate suppression of the cosmic star formation rate, since even after fresh gas infall is halted the gas already in galaxies continues to produce stars, and mergers among already-formed gas disks also trigger star formation. However, if the overlap phase of reionization is relatively gradual then there may be time for the suppression of star formation to become significant even before the end of overlap.

Once gas collects inside a halo and cools, it can collapse to high densities and form stars or a mini-quasar. Regardless of the nature of the source, its ability to form is determined by gas accretion which, in a hierarchical model of structure formation, is driven by mergers of dark matter halos. Therefore, in order to determine the lifetime of a typical source, we first define the age of gas in a given halo using the average rate of mergers which built up the halo. Based on the extended Press-Schechter formalism (Lacey & Cole 1993), for a halo of mass M at redshift z , the fraction of the halo mass which by some higher redshift z_2 had already accumulated in halos with galaxies is

$$F_M(z, z_2) = \text{Erfc} \left(\frac{1.69/D(z_2) - 1.69/D(z)}{\sqrt{2(S(M_{\text{min}}(z_2)) - S(M))}} \right), \quad (2)$$

where $D(z)$ is the linear growth factor at redshift z , $S(M)$ is the variance on mass scale M (defined using the linearly-extrapolated power spectrum at $z = 0$), and $M_{\text{min}}(z_2)$ is the minimum halo mass for hosting a galaxy at z_2 (as determined by the cutoff V_c which was discussed above). We define the total age of gas in the halo as the time since redshift z_2 where $F_M(z, z_2) = 0.2$, so that most (80%) of the gas in the halo has formed stars only since then. Thus, e.g., at $z = 6$ the age of the universe is 9.1×10^8 while the age of gas in a $3 \times 10^8 M_\odot$ halo is 3.6×10^8 yr ($z_2 = 8.8$), and the age of gas in a $10^{11} M_\odot$ halo is 5.5×10^8 yr ($z_2 = 12.0$). Low-mass halos form out of gas which has recently cooled for the first time, while high-mass halos form out of gas which has already spent previous time inside small galaxies. We emphasize that the age we have defined here is not the formation age of the halo itself, but rather it is an estimate for the total period during which the gas which is currently in the halo participated in star formation. However, the rate of gas infall is not constant, and even within the galaxy itself, the gas may not form stars at a uniform rate. The details involve complex astrophysics, so we account for the general possibility of bursting sources by adding a parameter ζ , the duty cycle. We pick a standard value of $\zeta = 0.25$, which implies that

each source is four times brighter during a lifetime which is four times shorter than the gas infall age that we specified above. This value of ζ is motivated by the fluctuating accretion rate seen in simulations, but in our model we allow for a wide range of possible values of ζ .

Consider an H II region produced by a source residing in a halo of total mass M and baryon fraction Ω_b/Ω_m . Since recombinations within the H II bubble are relatively unimportant, we assume that the radius of the bubble is close to the maximum radius r_{\max} that is simply determined by equating the number of ionized hydrogen atoms to the total number of ionizing photons produced by the source over its lifetime. We also assume for simplicity that each bubble is near its maximum size; this is a safe assumption for our purposes since the neutral fraction is relatively high at the outskirts of each H II bubble, and so the cross-section for observing a region with low optical depth is dominated by the central regions of the bubbles. To estimate the radius, we assume that the baryons in the halo are incorporated into stars with an efficiency of $f_{\text{star}} = 10\%$, and that the escape fraction for the resulting ionizing radiation is $f_{\text{esc}} = 5\%$, where this low escape fraction is understood to include the effect of recombinations in the dense gas within the source galaxy, its host halo, and the relatively dense immediate surroundings of the halo. If the stellar IMF is similar to the one measured locally (Scalo 1998) then ≈ 4000 ionizing photons are produced per baryon in stars (for a metallicity equal to $1/20$ of the solar value; Haiman, personal communication). We define a parameter which gives the overall number of ionizations per baryon,

$$N_{\text{ion}} \equiv 4000 f_{\text{star}} f_{\text{esc}} . \quad (3)$$

Denoting by \bar{n}_H^0 the present mean number density of hydrogen, the radius of the H II bubble is

$$r_{\max} = \frac{1}{1+z} \left(\frac{3}{4\pi} \frac{N_{\text{ion}}}{\bar{n}_H^0} \frac{\Omega_b}{\Omega_m} \frac{M}{m_p} \right)^{\frac{1}{3}} = 76 \text{ kpc} \left(\frac{7}{1+z} \right) \left(\frac{N_{\text{ion}}}{20} \frac{M}{10^9 M_\odot} \frac{0.148}{\Omega_m h^2} \right)^{\frac{1}{3}} . \quad (4)$$

Here and throughout this paper we use proper, not comoving, distances. Note that the radius r_{\max} is larger than the halo virial radius by a factor of ~ 20 that is almost independent of redshift and halo mass. Also note that we would obtain a similar result for the size of the H II region around a galaxy if we considered a mini-quasar rather than stars. This results from the high expected escape fraction for mini-quasars ($\sim 50\%$, e.g., Wood & Loeb 2000) which, together with the high radiative efficiency of $\sim 6\%$, overcomes the low efficiency ($\sim 0.2\text{--}0.6\%$, e.g., Magorrian et al. 1998) for incorporating the baryons in a galaxy into a central black hole.

2.2. Opacity of the IGM

Before the end of overlap, some large voids in the IGM are still neutral, and they completely block out the flux at the Ly α wavelength. However, even at a wavelength λ which corresponds to redshifted Ly α inside an H II region, the optical depth rises with redshift. There may in general be two sources of opacity at high redshift. First, the gas inside the H II region absorbs light strongly in the area of the resonance of the Ly α line, and can produce a significant opacity even with a very

small neutral hydrogen fraction. At higher redshifts, the mean density of the universe is higher, the voids are less empty because structure formation is still in its infancy, and the neutral fraction is higher since the ionizing intensity is lower. In addition, if the H II region is itself surrounded by still-neutral IGM then the damping wings of the Ly α line due to this neutral gas can be broad enough to produce a substantial opacity over the entire wavelength range corresponding to the H II region. Indeed, Miralda-Escudé (1998) showed that the neutral IGM can block out all H II regions up to a diameter of ~ 1 Mpc.

To determine the opacity, we begin with the standard (Gunn & Peterson 1965) opacity for absorption which includes the resonance,

$$\tau_{\text{GP}} = \frac{\pi e^2 f_{\alpha} \lambda_{\alpha} n_{\text{HI}}(z)}{m_e c H(z)} = 3.61 \times 10^5 \left(\frac{\Omega_b h}{0.0325} \right) \left(\frac{\Omega_m}{0.35} \right)^{-\frac{1}{2}} \left(\frac{1+z}{7} \right)^{\frac{3}{2}}, \quad (5)$$

for neutral gas at the mean density at redshift z . Here and throughout this paper we assume the high-redshift form for Hubble’s constant,

$$H(z) \approx H_0 \sqrt{\Omega_m} (1+z)^{\frac{3}{2}}, \quad (6)$$

where H_0 is Hubble’s constant at $z = 0$. More generally, gas at relative density $\Delta = \rho_g / \bar{\rho}_g$ and with a neutral fraction x_{HI} produces an optical depth

$$\tau_{\text{reson}} = \tau_{\text{GP}} x_{\text{HI}} \Delta, \quad (7)$$

where the subscript stands for resonance.

For the density distribution in the IGM within the H II bubble, we adopt the general picture (though not the full model) of Miralda-Escudé et al. (2000). This picture is based on the fact that voids can be quickly and easily ionized while the high recombination rate of dense clumps keeps them neutral. Thus, a rough description of the state of the IGM is that most of the gas up to some fiducial overdensity is ionized, and most of the gas above that overdensity is still neutral. Although the remaining neutral clumps can contain a significant gas mass, they take up only a small fraction of the volume and do not block a significant fraction of the ionizing radiation emanating from the central source. Thus the neutral clumps can essentially be ignored, and the total recombination rate is typically not high enough to limit the size of the H II bubble. Thus we describe the IGM within the large H II bubble as having an average density Δ relative to the mean, where it is understood that the ‘H II bubbles’ are not fully ionized since they contain a small volume of dense neutral clumps. Since the clumps are denser than average, the gas within the bubble which *is* ionized is characterized by a $\Delta < 1$. For the model of the density distribution used in Miralda-Escudé et al. (2000), if gas at $z = 6$ is ionized up to a density of 10 times the cosmic mean then the ionized gas has a $\Delta = 0.87$ and a clumping factor (i.e., mean value of density squared) of $C = 1.6$ times that for gas at the cosmic mean density. If the gas is ionized only up to a density of 2 times the cosmic mean then the numbers are $\Delta = 0.67$ and $C = 0.60$. Because of these relatively low clumping factors, an ionizing source can easily ionize the gas up to an overdensity of ~ 10 without sacrificing

many photons to balance recombinations. The actual maximum overdensity of ionized gas depends on the detailed geometry of the overdense regions and must vary with the distance from the source. Indeed, the model of Miralda-Escudé et al. (2000) is most accurate when the ionizing intensity in the IGM is uniform, and this is true only well after overlap; therefore, in this paper we instead use a model based on the H II bubbles of individual sources, a model which is much more accurate during overlap. We use the Miralda-Escudé et al. (2000) picture only in the limited sense of determining the effective value of Δ . An important detail is that while the size of the region that a given source can ionize depends essentially only on the mean Δ of ionized gas, the probability of observing a low optical depth in the region is particularly sensitive to the presence of the lowest-density voids. For the density distribution of Miralda-Escudé et al. (2000), only 0.9% of the mass, and 4.2% of the volume, is occupied by gas with $\Delta < 0.25$ at $z = 6$. The numbers are 7.6% of the mass and 25% of the volume, for $\Delta < 0.4$. In our calculations we thus use two different effective values of Δ ; we adopt as standard values $\langle \Delta \rangle = 0.8$ which is used to calculate the size of each bubble, and $\Delta_\tau = 0.4$ which is used to calculate the optical depth of the gas. Thus, e.g., the radius of the H II bubble [eq. (4)] is modified to

$$r_{\max} = 82 \text{ kpc} \left(\frac{7}{1+z} \right) \left(\frac{N_{\text{ion}}}{20} \frac{M}{10^9 M_\odot} \frac{0.148}{\Omega_m h^2} \frac{0.8}{\langle \Delta \rangle} \right)^{\frac{1}{3}}. \quad (8)$$

We assume ionization equilibrium for the hydrogen within the H II bubble. This is a safe assumption even though the recombination time for the IGM at $z = 6$ is around the Hubble time. Since equilibrium typically means a neutral fraction of $\sim 10^{-3}$ or less then the time to reach equilibrium is at most 10^{-3} of the recombination time. The recombination rate per volume is

$$\text{Rec rate} = \alpha_B (\bar{n}_H^0)^2 \frac{\Delta^2}{a^6}, \quad (9)$$

where $a = 1/(1+z)$ and the case B recombination coefficient for hydrogen at $T = 10^4$ K is $\alpha_B = 2.6 \times 10^{-13} \text{ cm}^3 \text{ s}^{-1}$. The ionization rate per volume is

$$\text{Ion rate} = x_{\text{HI}} \frac{dN_\gamma}{dt} \frac{1}{4\pi r^2} \bar{\sigma} \bar{n}_H^0 \frac{\Delta}{a^3}, \quad (10)$$

where $\bar{\sigma}$ is a frequency-averaged photoionization cross section, $\sim 2 \times 10^{-18} \text{ cm}^2$. We set $dN_\gamma/dt = N_\gamma/t_s$, where N_γ is the total number of ionizing photons produced (which equals the number of baryons in the halo times N_{ion}) and t_s is the source lifetime (see §2.1). Then the neutral fraction at radius r in the H II bubble is

$$x_{\text{HI}} = 3.15 \times 10^{-3} \left(\frac{t_s}{1.3 \times 10^8 \text{ yr}} \right) \left(\frac{r_{\max}}{82 \text{ kpc}} \right)^{-1} \left(\frac{\Delta_\tau / \langle \Delta \rangle}{0.5} \right) \left(\frac{r}{r_{\max}} \right)^2, \quad (11)$$

and the optical depth at Ly α caused by this gas is therefore

$$\tau_{\text{reson}} = 455 \left(\frac{1+z}{7} \right)^{\frac{9}{2}} \left(\frac{\Omega_m h^2}{0.148} \right)^{\frac{1}{2}} \left(\frac{\Omega_b h^2}{0.0211} \frac{t_s}{1.3 \times 10^8 \text{ yr}} \right) \left(\frac{N_{\text{ion}}}{20} \frac{M}{10^9 M_\odot} \right)^{-1} \left(\frac{\Delta_\tau}{0.4} \frac{r}{82 \text{ kpc}} \right)^2. \quad (12)$$

Note that the optical depth at a given radius depends on Δ_τ (by definition of Δ_τ), but it does not depend on r_{\max} (and thus on $\langle\Delta\rangle$), assuming that $r < r_{\max}$.

Our choice of duty cycle ζ affects the statistics of absorption not only through the lifetime $t_s \propto \zeta$; if, e.g., $\zeta = 0.25$, then for each active source with a highly ionized H II bubble there are three ‘dead’ bubbles, regions ionized by sources that have already turned off before $z = 6$. These bubbles have typically been dead for $\sim 2 \times 10^8$ yr, while the recombination time (if $\langle\Delta\rangle = 0.8$) is $\sim 2.5 \times 10^9$ yr. Thus, if the bubbles were initially highly ionized, at $z = 6$ they have a neutral hydrogen fraction below 10%. This fraction is high enough that the internal optical depth in these bubbles satisfies $\tau_{\text{reson}} \gg 1$, but the fraction is low enough that this gas does not contribute significant absorption through the Ly α damping wings. Thus, we treat the dead bubbles as neutral for the purpose of internal optical depth, but as fully ionized for the purpose of damping wings and in the calculation of the total filling factor of ionized gas in the universe.

2.3. Specific Predictions

In order to analyze the importance of the observations, we look for a specific property of the observed spectra that can be computed from our model. Although the mean optical depth declines with redshift, and this quantity is straightforward to determine observationally, we prefer to focus on the essential feature which defines Gunn-Peterson absorption. This is not the value of the mean optical depth, which is already rather high even at a somewhat lower redshift; the key feature is instead the presence of a long stretch of absorption which is continuous, i.e., which does not allow through any significant flux at all, even when observed with a very high spectral resolution. This feature also captures the physical difference between the IGM before and after reionization. At low redshift, observed spectra are characterized by overall transmission except for a dense forest of relatively narrow absorption lines corresponding to the cosmic web of sheets and filaments. The Ly α forest becomes denser with redshift, but as long as the low-density gas in the IGM is very highly ionized, a high-resolution spectrum should always show some transmission spikes, even when these spikes are rare and the mean optical depth is high. At redshifts approaching reionization, on the other hand, the IGM itself has a significant neutral fraction, and it produces continuous strong absorption over large redshift intervals. Before full reionization, parts of the IGM are neutral and they produce even longer intervals of total absorption.

From the previous subsections, our main parameters and their default values are the redshift $z = 6$, the minimum halo circular velocity $V_c = 16.5$ km/s of halos with galaxies, the relative density $\Delta_\tau = 0.4$ of ionized gas within the bubbles (where also $\langle\Delta\rangle = 2\Delta_\tau$), the overall source efficiency $N_{\text{ion}} = 20$, and the duty cycle $\zeta = 0.25$. For given parameter values, we calculate the total filling factor Q_{II} of H II bubbles, which is simply the integral of halo number density times the maximum ionized volume $4\pi r_{\max}^3/3$ due to each halo. We emphasize that the volume taken up by H II bubbles includes the small volume fraction of neutral clumps which remain within each bubble. The end of the overlap stage of reionization corresponds to $Q_{\text{II}} = 1$, because at this point

all the low-density gas is ionized. We allow Q_{II} to be greater than unity in the post-overlap stage, where, e.g., a value of $Q_{\text{II}} = 5$ means that the total number density of ionizing photons produced by all sources is five times greater than the mean number density of hydrogen atoms in the IGM (where the dense neutral clumps are not included). For direct comparison with observations, we compute also the mean free path λ_{GP} for observing a region with optical depth less than a given $\tilde{\tau}$. We deal with the mean free path, a statistical quantity, since the ionizing intensity in the IGM is extremely inhomogeneous during reionization. At redshift z , we have

$$\lambda_{\text{GP}} = \left[\int_{M_{\text{min}}}^{\infty} \sigma_{\tilde{\tau}}(M) \frac{dn}{dM} dM \right]^{-1}, \quad (13)$$

where $n(M)$ is the proper number density of halos with mass up to M , and $\sigma_{\tilde{\tau}}(M)$ is the cross-section for intersecting some point with a Ly α optical depth less than $\tilde{\tau}$ along a line of sight through the H II bubble produced by a halo of mass M . The mass M_{min} is determined by the halo with the minimum V_c or, if it is bigger, by the smallest halo whose H II bubble is large enough to produce some point with $\tau < \tilde{\tau}$. In a stretch of length l along a random line of sight, the average intersected number of H II bubbles with a $\tau < \tilde{\tau}$ region is l/λ_{GP} . Also, the chance of not intersecting any such bubble in the same stretch is $\exp[-l/\lambda_{\text{GP}}]$. We can similarly calculate a mean free path for encountering any ionized gas, regardless of the optical depth:

$$\lambda_{\text{II}} = \left[\int_{M_{\text{min}}}^{\infty} \sigma_{\text{II}}(M) \frac{dn}{dM} dM \right]^{-1}, \quad (14)$$

where in this case M_{min} is always set by the cutoff V_c , and $\sigma_{\text{II}}(M) = \pi r_{\text{max}}^2$. It is also easy to show that a fraction Q_{II} of a random line of sight is covered by some part of an H II bubble, so on average a stretch of length λ_{II} intersects one bubble with a typical intersected path of length $Q_{\text{II}}\lambda_{\text{II}}$.

In order to obtain λ_{GP} , we must first calculate the optical depth of every parcel of gas. To calculate the optical depth at each point within an H II bubble at redshift z we add τ_{reson} to the optical depth caused by the red damping wings of neutral IGM at lower z and the blue damping wings of neutral IGM at higher z . We include the blue damping wings since we are considering here bubbles along the line of sight to a given source (e.g., a quasar), and are not considering the region ionized by the quasar itself (i.e., the proximity effect). The optical depth is given by an integral along the line of sight of the number density of neutral hydrogen times the scattering cross-section of the Ly α line. Consider at high redshift a stretch of IGM at the cosmic mean density which has a neutral fraction x_{HI} and is located between redshifts z_1 and z_2 . On light with an observed wavelength $\lambda = \lambda_{\alpha}(1+z)$, this gas produces through the damping wing an optical depth of (Miralda-Escudé 1998)

$$\tau_{\text{damp}} = 6.43 \times 10^{-9} x_{\text{HI}} \tau_{\text{GP}} \left[\text{I} \left(\frac{1+z_2}{1+z} \right) - \text{I} \left(\frac{1+z_1}{1+z} \right) \right], \quad (15)$$

where τ_{GP} is given by eq. (5) and

$$\text{I}(x) \equiv \frac{x^{9/2}}{1-x} + \frac{9}{7}x^{7/2} + \frac{9}{5}x^{5/2} + 3x^{3/2} + 9x^{1/2} - \frac{9}{2} \ln \left| \frac{1+x^{1/2}}{1-x^{1/2}} \right|, \quad (16)$$

and we have assumed $z < z_1 < z_2$ or $z_1 < z_2 < z$ so that the absorption does not involve the central region of the Ly α line, near resonance.

The optical depth produced by an IGM with a given filling factor Q_{II} depends on the distribution of neutral and ionized regions within the IGM. When $Q_{\text{II}} \geq 1$ we assume that there is no neutral IGM and that $\tau_{\text{damp}} = 0$. In this case, not only is there no neutral IGM, but also most points in the IGM feel the radiation from more than one source. As a simple way of accounting approximately for the high number density of sources, for each source we consider its bubble only out to radius $r_{\text{max}}/\sqrt{Q_{\text{II}}}$, since the more distant gas is likely to be closer to some other source, given that $Q_{\text{II}} > 1$. Note that we are still assuming that the radiation intensity at each point is dominated by the nearest source; we discuss this issue further in §4.

When $Q_{\text{II}} < 1$, τ_{damp} depends on the exact distribution of neutral and ionized gas on both sides of a given H II bubble. It is not possible to analytically describe the full complexity of this distribution, so we use the statistical properties of this distribution in order to get a handle on the expected range of values of τ_{damp} . Specifically, we know the volume-averaged neutral fraction $x_{\text{HI}} = 1 - Q_{\text{II}}$, and we also know that on average a stretch of length λ_{II} intersects a single bubble with a typical intersected path of length $Q_{\text{II}}\lambda_{\text{II}}$ [see equation (14)]. We therefore adopt the following simple model for the IGM on each side of the H II bubble, along a given line of sight: We take two consecutive segments of length λ_{II} each, where in each segment the central length of $Q_{\text{II}}\lambda_{\text{II}}$ is ionized and the rest is neutral. After these two segments, we simply take a uniform IGM with the neutral fraction set equal to $1 - Q_{\text{II}}$. The optical depth is only weakly dependent on the precise redshift at which this neutral IGM is cut off, so we fix a minimum $z = 4$ and a maximum $z = 12$ (i.e., we do not consider sources observed at $z > 12$). By trying other possible arrangements of neutral gas within the IGM we find a typical systematic uncertainty of around a factor of two in λ_{GP} (when $Q_{\text{II}} < 1$); the particular arrangement of segments that we have chosen is arbitrary, except that it gives results that lie in the central range of values obtained from various possible arrangements.

To illustrate some numerical values, since with our standard parameters $Q_{\text{II}} = 5.0$ we consider here an example with $z = 8$, $N_{\text{ion}} = 10$ and $V_c = 40$ km/s, for which $Q_{\text{II}} = 0.39$. In this case, $\lambda_{\text{II}} = 0.29$ Mpc. Consider, for example, a $10^{11}M_{\odot}$ halo, which produces an $r_{\text{max}} = 0.24$ Mpc; if a line of sight passes at a projected radius of 0.05 Mpc from the center of this bubble, the total length through the H II bubble is 0.46 Mpc. At the center of this line through the bubble, the optical depth is 11.1, made up of $\tau_{\text{reson}} = 5.6$ and $\tau_{\text{damp}} = 2.7$ and 2.8 from the red and blue damping wings, respectively. Note that in calculating the damping wings we have neglected the possibility that they could be affected by density fluctuations or peculiar velocities in the neutral gas. The overall τ_{damp} results mainly from the integrated effect of a length of ~ 0.5 Mpc of neutral gas. At $z = 6$, the typical $1 - \sigma$ density fluctuation on this scale is 0.32, so fluctuations are likely to have only a moderate effect on the overall statistics, but the effect is significant and should be studied. The damping wings block out small bubbles and imply that typically, when $Q_{\text{II}} < 1$, transmitted flux is possible only through bubbles produced by halos of mass at least $\sim 10^{11}\text{--}10^{12}M_{\odot}$. This

permits a rough estimate of λ_{GP} in this case. Indeed, if $\zeta = 0.25$ then at $z = 6$ the number density of active bubbles produced by halos with $M > 10^{11} M_{\odot}$ is ~ 0.1 per Mpc^3 . Each bubble has an $r_{\text{max}} \sim 0.4$ Mpc, so if each bubble produces a low optical depth out to a projected radius of $r_{\text{max}}/2$, then $\lambda_{\text{GP}} \sim 80$ Mpc. This explains the high values of λ_{GP} found in the next section whenever $Q_{\text{II}} < 1$.

3. Results

To compare our model with the observations, we first note the sizes of the widest dark regions found in the quasar spectra. Becker et al. (2001) found a dark region at $z = 5.87\text{--}6.15$, or 16.8 Mpc (considering just $\text{Ly}\alpha$, not $\text{Ly}\beta$), and Djorgovski et al. (2001) found a dark region at $z = 5.25\text{--}5.31$, or 4.7 Mpc. In both cases, the highest transmission spikes within these regions correspond to $\tau \sim 2$, but measurement noise may well explain these spikes. More quantitatively, within the dark region Djorgovski et al. (2001) estimate a mean flux level of 1.6×10^{-3} relative to the quasar continuum, and a standard deviation of ~ 0.01 per resolution element (which is ~ 10 pixels). Since there are ~ 50 resolution elements within the dark interval, both of these numbers imply that the upper limit on the flux within a single resolution element corresponds to $\tau \sim 2.5$. As our default value we adopt this limit of $\tilde{\tau} = 2.5$, i.e., we assume that even a small stretch with $\tau < 2.5$ can be excluded within the dark regions in both of the observed spectra. Figure 1 shows the predicted values of λ_{GP} and Q_{II} as a function of the cutoff halo circular velocity V_c , for several redshifts between $z = 5$ and $z = 10$. For our standard parameters ($V_c = 16.5$ km/s at $z = 6$), we find $\lambda_{\text{GP}} = 13.3$ Mpc and $Q_{\text{II}} = 5.0$. At a given redshift, Q_{II} declines more steeply with V_c at high values of V_c , because the halo mass function declines steeply at high mass values which correspond to very rare halos. At low V_c , λ_{GP} depends only weakly on the cutoff since even when $Q_{\text{II}} > 1$ the total cross-section of low- τ regions in H II bubbles is dominated by bubbles due to relatively massive halos. When the minimum V_c is increased, as Q_{II} drops below 1 there is a steep rise in λ_{GP} due to the effects of the damping wings of the neutral IGM.

Figure 2 shows the dependence of λ_{GP} and Q_{II} on Δ_{τ} and on $\tilde{\tau}$. In every case we set $\langle \Delta \rangle = 2\Delta_{\tau}$, except that $\langle \Delta \rangle$ is not increased past unity. In general, a lower $\langle \Delta \rangle$ makes it easier to reach the end of overlap, since a greater mass fraction of the gas remains in neutral clumps which do not need to be ionized in order to reach $Q_{\text{II}} = 1$. A lower Δ_{τ} lowers τ_{reson} at a given radius in a bubble in proportion to Δ_{τ}^2 , where one factor of Δ_{τ} is due to the reduced neutral fraction. The plot of λ_{GP} as a function of $\tilde{\tau}$ indicates that a more detailed comparison should be possible in the future between theory and observation. Indeed, the full probability distribution of τ as a function of redshift, and the correlation function of τ along the line of sight, should be compared between detailed observations and detailed numerical simulations with accurate radiative transfer.

Figure 3 shows the dependence of λ_{GP} and Q_{II} on the source parameters N_{ion} and ζ . Increasing N_{ion} causes a proportional increase in Q_{II} , since a greater number of ionizing photons is produced. At the same time, λ_{GP} decreases since the ionizing intensity increases at a given distance from

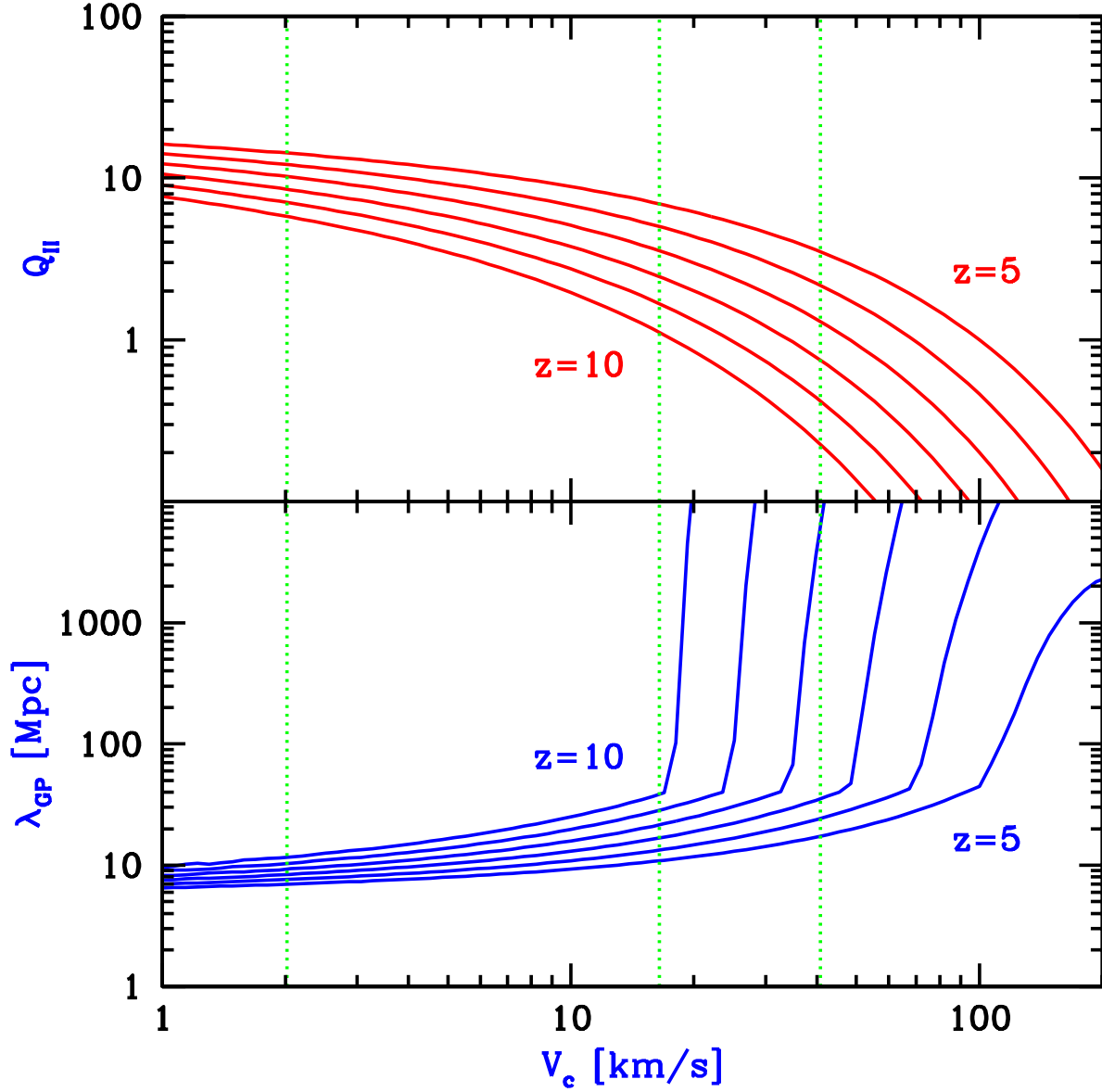


Fig. 1.— The mean free path λ_{GP} and the filling factor Q_{II} versus the minimum circular velocity V_c for halos which host galaxies. The bottom panel shows the mean free path for crossing through a region with a Ly α optical depth less than $\bar{\tau} = 2.5$. The mean free path in proper Mpc is shown versus the cutoff, minimum halo circular velocity V_c in km/s. The upper panel shows the H II filling factor versus V_c . In both panels, the different curves correspond to redshifts 5, 6, 7, 8, 9, and 10, as indicated. Vertical dotted lines show the values of V_c that correspond roughly to H_2 cooling (2.0 km/s), atomic cooling (16.5 km/s), and pressure suppression (41 km/s). Other parameter values are $\Delta_\tau = 0.4$, $\langle \Delta \rangle = 0.8$, $N_{\text{ion}} = 20$, and $\zeta = 0.25$.

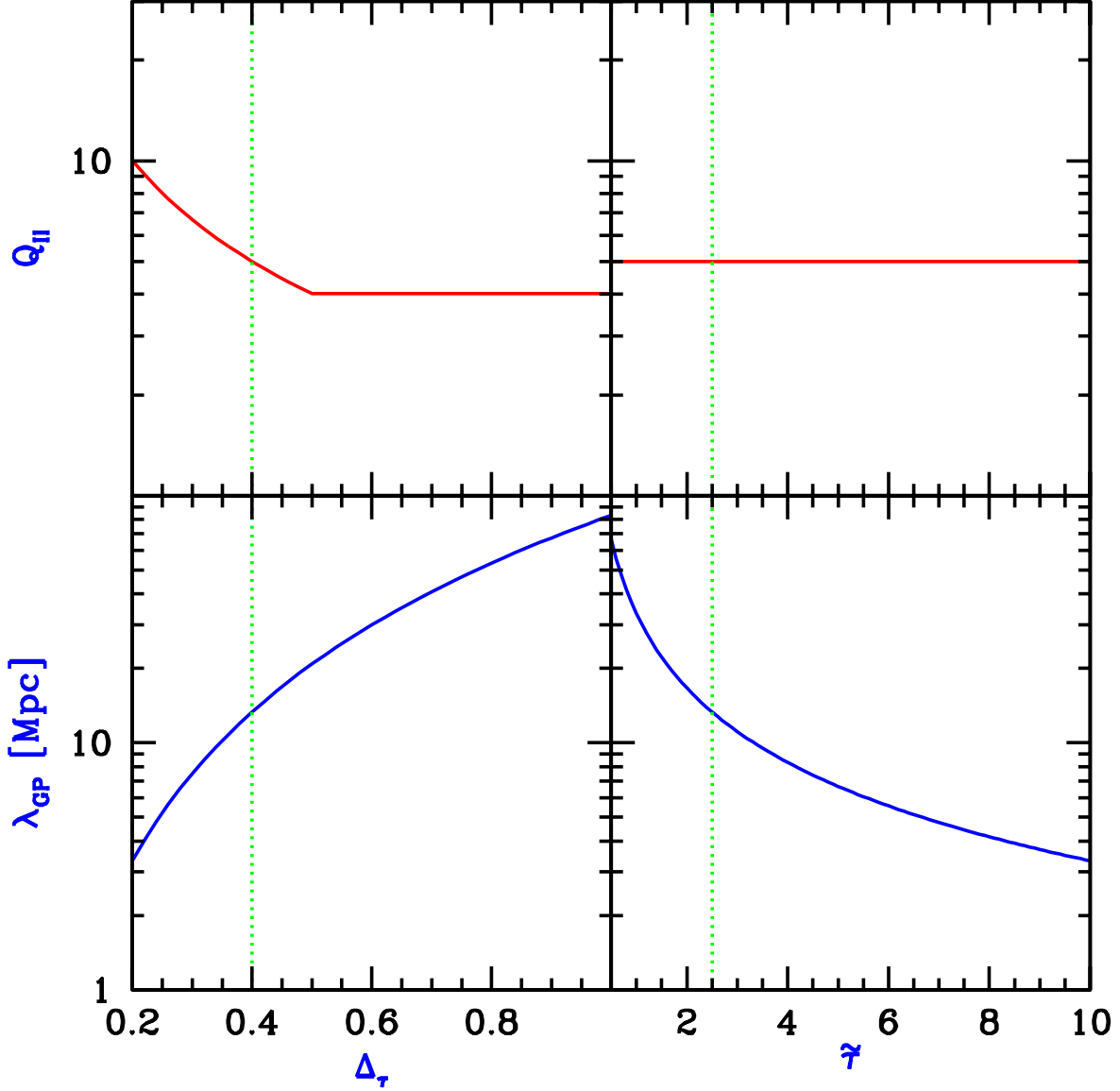


Fig. 2.— The mean free path λ_{GP} and the filling factor Q_{II} . Bottom panels show the mean free path in proper Mpc for crossing through a region with $\tau < \tilde{\tau}$. Upper panels show the H II filling factor. In the left panels, the gas density Δ_τ is varied, where $\Delta = \rho/\bar{\rho}$. In every case we set $\langle\Delta\rangle = 2\Delta_\tau$, except that $\langle\Delta\rangle$ is not increased past unity. The vertical dotted line shows our standard value of $\Delta_\tau = 0.4$. In the right panels, the maximum optical depth $\tilde{\tau}$ is varied. The vertical dotted line shows our standard value of $\tilde{\tau} = 2.5$. Other parameter values are $z = 6$, $V_c = 16.5$ km/s, $N_{\text{ion}} = 20$, and $\zeta = 0.25$.

a source. As before, λ_{GP} increases sharply if N_{ion} is lowered to the point where $Q_{\text{II}} < 1$. The duty cycle does not affect Q_{II} since we assume that the bubbles of dead sources remain ionized. Each active bubble is more highly ionized when ζ is small, but only bubbles with active sources can have a low optical depth, so a low ζ leads to a slight increase in λ_{GP} . The dependence on ζ is weak also when parameters are chosen so that $Q_{\text{II}} < 1$. Given this weak dependence, Q_{II} and λ_{GP} are also expected to be insensitive to clustering of sources. Consider a simple toy model for clustering in groups of $N > 1$ halos, where we make each source N times brighter but assume N times fewer sources. As before, Q_{II} remains unchanged, but each bubble becomes bigger and more highly ionized at a given radius. Indeed, the radius at which we find a given τ_{reson} goes up as \sqrt{N} , so the cross-section goes as $r^2 \propto N$, which cancels out the $1/N$ decrease in the density of sources. Thus, when $Q_{\text{II}} > 1$ clustering has almost no effect on λ_{GP} , but it does decrease λ_{GP} somewhat when $Q_{\text{II}} < 1$, since damping wings have a smaller effect on larger bubbles. Note that even parameters that do not change λ_{GP} significantly *can* be probed with detailed observations since they do change ionized gas fractions within H II bubbles as well as the distribution of bubble sizes.

The discussion so far shows that after considering a wide range of parameter values we expect the universe to be well past the end of overlap by redshift six. However, present observations place only weak direct constraints on the parameters controlling the abundance and efficiency of sources at such high redshifts. Thus, our goal is to use directly the observations of wide regions of Gunn-Peterson absorption to infer the state of reionization at $z = 6$, regardless of the precise parameter values. To this end, Figure 4 shows a scatter plot of points derived from the entire parameter space of reasonable values. Shown are 5000 points, where each corresponds to a set of parameters selected randomly from the ranges $z = 5\text{--}10$, $V_c = 1\text{--}200$ km/s, $\Delta_\tau = 0.2\text{--}1$, $N_{\text{ion}}=2\text{--}200$, and $\zeta = 0.01\text{--}1$. We hold $\tilde{\tau} = 2.5$ fixed, and choose parameters from uniform distributions in the log (except for z). In the figure we also mark with an \times the location corresponding to our standard parameter values, and we draw a straight line at $Q_{\text{II}} = 1$. The figure clearly illustrates that over a broad range of possible parameter values, there is a very strong correlation between Q_{II} and λ_{GP} . Indeed, for most parameter values we find that $\lambda_{\text{GP}} < 100$ Mpc if and only if $Q_{\text{II}} > 1$. Thus, when $Q_{\text{II}} < 1$ the incidence of transparent regions should become very low, since for example $z = 6\text{--}7$ corresponds to a line-of-sight length of only 51 Mpc. Thus, e.g., if $\lambda_{\text{GP}} = 1000$ Mpc then the chance of encountering any $\tau < 2.5$ spot along a given line of sight is about 1 in 20. Note also that while the y -axis in the figure is shown only up to $\lambda_{\text{GP}} = 10^4$ Mpc, most of the points at $Q_{\text{II}} < 1$ actually lie at even higher values of λ_{GP} .

The appearance of Figure 4 is determined by the various input parameters whose individual effects were shown in the previous figures. If V_c is varied from small to large values, with all other parameters fixed, the result is a single curve which goes from the top left to the bottom right corner in the figure. Such curves drawn at various redshifts all lie almost on top of each other at $Q_{\text{II}} > 1$, but at $Q_{\text{II}} < 1$ the redshift dependence explains almost all of the scatter in the figure; in fact, if we used only $z > 6$ instead of $z > 5$, there would be significantly less scatter at $Q_{\text{II}} < 1$, with the

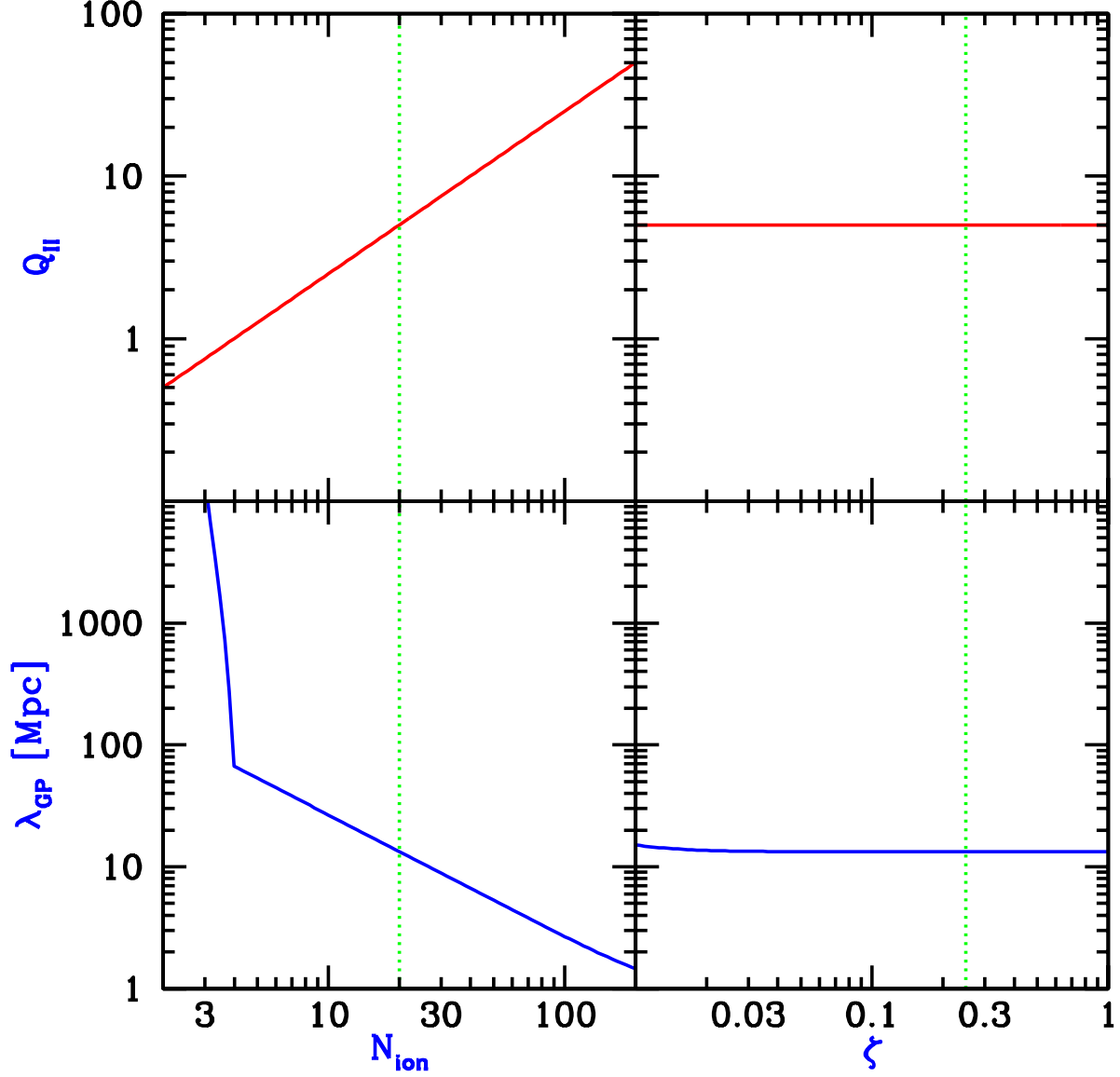


Fig. 3.— The mean free path λ_{GP} and the filling factor Q_{II} . Bottom panels show the mean free path in proper Mpc for crossing through a region with a Ly α optical depth less than $\bar{\tau} = 2.5$. Upper panels show the H II filling factor. In the left panels, the source efficiency N_{ion} is varied. The vertical dotted line shows our standard value of $N_{\text{ion}} = 20$. In the right panels, the source duty cycle ζ is varied. The vertical dotted line shows our standard value of $\zeta = 0.25$. Other parameter values are $z = 6$, $V_c = 16.5$ km/s, $\Delta_\tau = 0.4$, and $\langle \Delta \rangle = 0.8$.

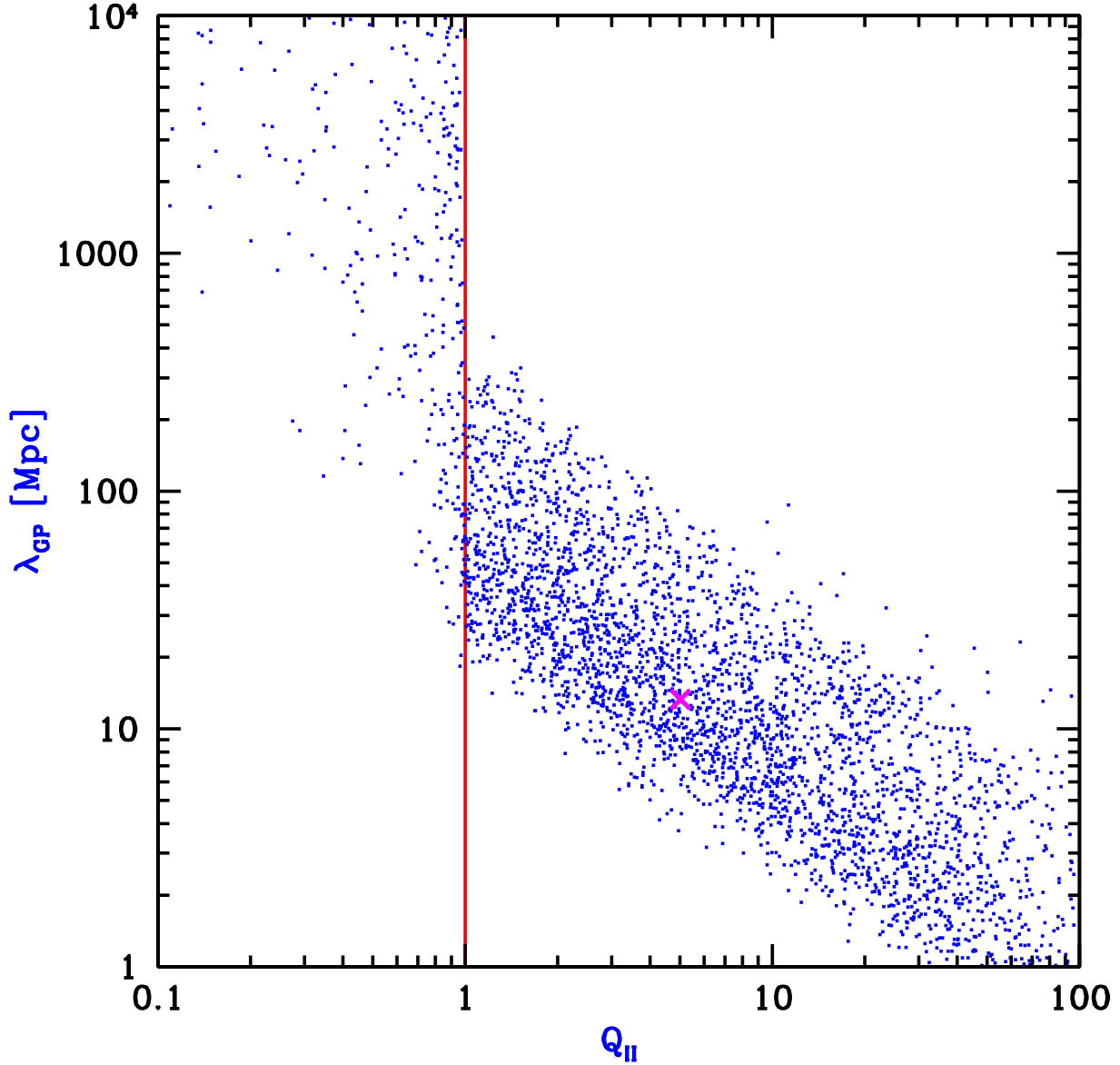


Fig. 4.— The mean free path λ_{GP} versus the filling factor Q_{II} . The vertical axis is the mean free path in proper Mpc for crossing through a region with a Ly α optical depth less than $\bar{\tau} = 2.5$. The horizontal axis shows the H II filling factor. The scattered points show the results from 5000 sets of parameters selected randomly from the parameter ranges shown in figures 1, 2, and 3 (except that $\bar{\tau} = 2.5$ is held fixed). The large \times marks the point corresponding to our standard parameter values. The solid vertical line is drawn at $Q_{\text{II}} = 1$.

points sticking closer to the vertical line $Q_{\text{II}} = 1$. In order to be conservative we also varied Δ_τ over a wide range, and this parameter is responsible for most of the scatter at $Q_{\text{II}} > 1$. As for the other parameters, variations in the source efficiency N_{ion} can be responsible for only a minor fraction of the apparent scatter; finally, varying ζ has little effect on the figure.

By any reasonable definition of pre-overlap, bubbles of transmitted flux should be extremely rare during pre-overlap. For a given filling factor $Q_{\text{II}} < 1$, the probability that a given point is inside at least one bubble is Q_{II} , if the point is chosen uniformly over volume. If we make the approximation that different bubbles are independently placed then the probability of a given point being in exactly one bubble is $Q_{\text{II}} \exp[-Q_{\text{II}}]$. Thus, the probability that a given point is in two or more overlapping bubbles is

$$P_{\text{over}} = Q_{\text{II}} [1 - e^{-Q_{\text{II}}}] . \quad (17)$$

Pre-overlap can be defined as the time when $P_{\text{over}} \ll 1$. For example, $P_{\text{over}} = 0.1$ when $Q_{\text{II}} = 0.34$ and $P_{\text{over}} = 0.01$ when $Q_{\text{II}} = 0.10$.

4. Discussion

In the previous section we showed that over a broad range of possible parameters that characterize the IGM and the population of ionizing sources, there is a strong correlation between the reionization state of the IGM as measured by Q_{II} and the typical observed length of Gunn-Peterson absorption λ_{GP} . We now consider the recent spectral observations in light of these results. Both the 16.8 Mpc dark region at $z = 6$ (Becker et al. 2001) and the 4.7 Mpc dark region at $z = 5.3$ (Djorgovski et al. 2001) most likely correspond to $Q_{\text{II}} > 1$. If indeed true, this means that these observations correspond to post-overlap just like observations at lower redshift, but their novelty comes from the approach toward overlap which implies that the voids, while being mostly ionized, still contain a high enough neutral fraction to produce wide regions of high optical depth in spectra. The $z = 5.3$ observation cannot correspond to $Q_{\text{II}} < 1$, since there are regions of high transmitted flux at still higher redshifts in the same spectrum, while Q_{II} is expected to increase with time (see Figure 1), and $Q_{\text{II}} < 1$ should correspond to a spectrum that is almost completely dark except for the proximity effect of the quasar (see Figure 4). Note also that we have selected the 4.7 Mpc region at $z = 5.3$ as the widest dark region over the range $z = 5.2$ – 5.6 , which measures 30 Mpc. This selection effect means that the length of 4.7 Mpc must be a few times larger than the effective λ_{GP} over this redshift range. In contrast, the $z = 6$ observation may in fact imply the discovery of the IGM during overlap, since the dark region is observed right up to the region affected directly by the quasar emission. Clearly, however, a dark region of ~ 50 Mpc must be observed before we can conclude that we are likely observing the effects of damping wings and of the $Q_{\text{II}} < 1$ era. Alternatively, if 15 Mpc dark regions are observed at $z = 6$ along many lines of sight, with the dark regions always extending right up to the zone of the proximity effect of the quasar, this also will constitute strong evidence that the end of overlap has been observed.

We now consider an additional argument which deals with an aspect of reionization that has not been included thus far. We examine the effect of the increasing intensity due to multiple sources reaching every point within overlapping bubbles. This also has implications for the amount of time after the end of overlap during which wide regions of Gunn-Peterson absorption can still be observed. We embark on this discussion in order to understand an additional implication of the recent observations, which is a result of the significant differences between the spectra along the two lines of sight. We argue that the observations are inconsistent with a rapid, homogeneous overlap era, and that this presents an important challenge to theoretical models.

The end of overlap ($Q_{\text{II}} = 1$) marks the first time when all gas in voids can see at least one ionizing source. Thus, as long as $Q_{\text{II}} < 1$, some voids are still completely neutral and they block the radiation from some ionizing sources. The last stages of overlap should occur within a small fraction of a Hubble time at the overlap redshift, since each source is required to ionize only the region out to its nearest neighbors, which are likely to be fairly nearby. In addition, the photons which gradually succeed in ionizing the dense surroundings of each galaxy during pre-overlap then find it very easy to ionize the low-density voids during overlap. Each time two or more bubbles are joined, the gas within the combined volume is exposed to the ionizing radiation from more than one source. Therefore, the ionizing intensity inside H II regions begins to rise, allowing those regions to expand into high-density gas which had previously recombined fast enough to remain neutral when the ionizing intensity had been low. Since each bubble coalescence accelerates the process of reionization, the overlap phase has the character of a phase transition and should occur rapidly.

At the end of overlap, the final shadows cast by neutral gas in voids disappear, and every point in the IGM can begin to see all ionizing sources in the universe, except that two barriers must still be overcome. One barrier is simply due to the light travel time. At redshift z , the ionizing intensity at a given point is determined by taking the number density of sources times the flux of each source, and integrating over a spherical volume element out to a radius r . The flux of each source is given by its intensity divided by r^2 . The intensity of each source is proportional to the halo mass, times an efficiency factor, divided by the source lifetime. If we use for the purposes of this estimate the approximate assumption that all sources have the same lifetime, then the result depends only on an integral of halo mass times number density, i.e., on the total collapse fraction F_{col} , which is the mass fraction contained in halos which host galaxies. Note that we can set $\zeta = 1$ since a smaller duty cycle increases the intensity of each source but decreases the number density of sources by the same factor. For gas of relative density Δ_τ , the optical depth which results from integrating sources out to radius r is

$$\tau_{\text{reson}} = 9.78 \left(\frac{1+z}{7} \right)^{\frac{3}{2}} \left(\frac{\Omega_m h^2}{0.148} \right)^{-\frac{1}{2}} \left(\frac{\Omega_b h^2}{0.0211} \frac{t_s/\zeta}{5 \times 10^8 \text{ yr}} \right) \left(\frac{N_{\text{ion}} F_{\text{col}}}{20 \cdot 0.15} \right)^{-1} \left(\frac{\Delta_\tau}{0.4} \right)^2 \left(\frac{r}{\text{Mpc}} \right)^{-1}. \quad (18)$$

The result that the optical depth approaches 0 when r is large arises from the proportionality of the total intensity to the radius r . This divergence of intensity with distance is well known from Olber's paradox, which applies here since we are considering a small region and ignoring redshift

effects. This simple estimate implies that if the light travel time were the only barrier, gas in voids would reach $\tau < 2.5$ in 13 Myr, and $\tau < 1$ in 32 Myr. These numbers can be increased by making sources less efficient (i.e., decreasing N_{ion}) or by making high-mass halos dominate over low-mass ones. As mentioned in §2.1, one natural process which increases V_c is the suppression of gas infall into low-mass halos. This suppression may already be important at the end of overlap, and if it raises V_c from 16.5 km/s to 41 km/s then F_{col} at $z = 6$ decreases from 0.15 to 0.066, increasing the light travel time needed to reach $\tau < 2.5$ by a factor of 2.3. If future observations discover that star formation at high redshift occurs efficiently only in galaxies with $V_c = 100$ km/s or greater, then the light travel time will be increased by an additional factor of 4.7 beyond the effects of pressure suppression. In addition, although we have used the fiducial value $\Delta_\tau = 0.4$ in the estimate of the optical depth, in this context we are particularly sensitive to voids which have a relatively low underdensity and therefore still produce wide regions of Gunn-Peterson flux. If we find a void with $\Delta_\tau = 0.8$, then in this region the light travel time is increased by a factor of 4.

The second barrier to increasing the ionizing intensity comes from the shadow due to the small volume of gas which remains in neutral clumps even during post-overlap. As in the discussion at the beginning of §2.2, we adopt here the model of Miralda-Escudé et al. (2000) for the density distribution in the IGM and also for the resulting mean free path of ionizing photons. In this model, if gas at $z = 6$ is ionized up to a density of 10 times the cosmic mean then the ionized gas has a clumping factor of $C = 1.6$ times that for gas at the cosmic mean density, and the mean free path is 2.9 Mpc. If the gas is instead ionized up to 100 times the cosmic mean density then $C = 4.5$ and the mean free path is 33 Mpc. Thus, the remaining shadow of neutral regions may temporarily prevent the intensity from increasing rapidly, at least until most of the gas in filaments with moderate overdensities is ionized. A different way to get a similar result is to extrapolate to high redshift the absorption due to the Ly α forest; Becker et al. (2001) find that this implies an overall average optical depth of ~ 2 –3 at $z = 5.3$, and this fairly high value implies a shadow that must keep the ionizing intensity from increasing rapidly.

An important role in delaying the end of the Gunn-Peterson trough may be played by the population of photo-evaporating halos. If molecular hydrogen is dissociated, as discussed above, then galaxies around the time of overlap form only in halos above $\sim 10^8 M_\odot$, where atomic cooling is efficient. However, most of the gas which lies in halos is inside smaller halos (down to $\sim 10^5 M_\odot$), where the lack of cooling prevents the formation of galactic disks and stars or mini-quasars. Barkana & Loeb (1999) showed that photoionization heating by the cosmic UV background (or shock heating; Cen 2001) could then evaporate much of this gas back into the IGM, with the process beginning during overlap. They showed that this process affects a broad range of halo masses, with only a small gas fraction evaporating out of $10^8 M_\odot$ halos, but with halos below $\sim 10^6 M_\odot$ losing their entire gas content because of their shallow gravitational potential wells. For overlap at $z \sim 6$, around 20% of the gas in the universe undergoes this photo-evaporation process, and this gas represents most of the gas which is already in halos just before overlap. Gas in the smallest halos evaporates very quickly into the IGM, but the larger halos which retain some of their gas expand only gradually,

and may cast a shadow for some time, preventing ionizing photons from reaching large distances. These surviving halos may also contribute to the high column density end of the Ly α forest at $z \sim 3$ (Bond, Szalay, & Silk 1988; Abel & Mo 1998).

The process of reionization may be very inhomogeneous, with overlap occurring at substantially different times in different places. Such inhomogeneity can be enhanced due to variations in the IGM density, clustering of sources, and spatial or temporal variation in source parameters such as the efficiency N_{ion} . Still, a large inhomogeneity is unlikely if the relatively common low-mass halos dominate. Taking the cooling mass as the lower mass limit at $z = 6$, for instance, there are 3000 halos per Mpc^3 . The number density is 130 per Mpc^3 for $V_c = 41$ km/s, and 3 per Mpc^3 for $V_c = 100$ km/s. Thus, if the efficiency N_{ion} is high only in high-mass halos, then strong Gunn-Peterson absorption can last down to lower redshift, because there are fewer stars in galaxies (i.e., F_{col} is smaller), because reionization is more inhomogeneous, and because the bubble around each individual source must grow very large and thus the source must overcome a strong shadow due to neutral clumps within the bubble. Whatever the explanation, the two recent observations together imply that the increase in the ionizing intensity during post-overlap must have been gradual, or that overlap must have occurred inhomogeneously. This follows from the fact that overlap in one line of sight occurs at $z > 5.9$, while a relatively large region of strong absorption is found along a second line of sight at $z = 5.3$, and the age difference between these redshifts is large (140 Myr). This significant cosmic variance, which has been observed even with only two lines of sight, further justifies the statistical approach that we adopted in §2.3, where we opted to study λ_{GP} rather than the mean optical depth.

Note that the the ionizing intensity starts to increase in overlapping bubbles even when $Q < 1$, but this effect should be significant only in the short period when Q approaches unity. Furthermore, when Q is significantly less than unity any transmitted flux must be very rare since the damping wings block out flux from most bubbles very effectively, almost regardless of the source parameters.

5. Conclusions

We have constructed a model of reionization in order to interpret recent observations of strong absorption in quasar spectra. By taking the H II bubble produced by each ionizing source, and considering the statistics of the ensemble of these bubbles, we have derived for given source parameters the filling factor Q_{II} of H II in the IGM, and the mean free path λ_{GP} for observing a region with optical depth less than a given $\tilde{\tau}$. In particular, we expect the universe to be well past the end of overlap by redshift six, with a $\lambda_{\text{GP}} \sim 10$ Mpc. However, regardless of the source parameters, we find a strong correlation between the reionization state of the IGM as measured by Q_{II} and the typical observed length of Gunn-Peterson absorption λ_{GP} . We conclude that the post-overlap era is consistent with the observed dark regions of 16.8 Mpc at $z = 6$ (Becker et al. 2001) and 4.7 Mpc at $z = 5.3$ (Djorgovski et al. 2001). The $z = 5.3$ observation cannot correspond to $Q_{\text{II}} < 1$, since the universe before the end of overlap should correspond to a spectrum that is almost com-

pletely dark except for the proximity effect of the quasar. This strong absorption results from the damping wings of neutral IGM, which block out the flux from all except very large, and rare, H II bubbles. The $z = 6$ observation is consistent with the state of the IGM before the end of overlap, since the dark region extends right up to the highest available redshift. If this interpretation is the correct one then much wider dark regions are expected and should be revealed by spectra of even higher-redshift sources. Alternatively, the discovery of the reionization era can be established even with quasars at $z \gtrsim 6$ if multiple lines of sight all show Gunn-Peterson absorption.

Combining the two recent observations constrains the evolution of the ionizing intensity during and after overlap. The observations imply that along one line of sight, overlap occurs at $z > 5.9$, while a relatively large region of strong absorption is found along a second line of sight at $z = 5.3$. The age difference between these redshifts is 140 Myr, which is much longer than our estimate of the light travel time needed to make the voids transparent due to the combined intensity of multiple ionizing sources. Thus, the ionizing intensity during post-overlap must have increased gradually, with a delay caused by the shadows due to the remaining neutral clumps. The neutral gas in halos which photo-evaporated during and after overlap may also have cast a significant shadow. If reionization was dominated by relatively high-mass, rare halos, then overlap occurred inhomogeneously, and this can also help to explain the observations.

In this paper we have planted the initial seeds of a very rich phenomenological field. Observers and theorists should calculate and compare the probability distribution of τ as a function of redshift, and the correlation function of τ along the line of sight. These statistical quantities will contain information on the size distribution of H II bubbles, on the neutral fraction distribution within the bubbles, and on the density distribution of neutral IGM outside the bubbles. This emerging field will benefit from measurements of increasing resolution and signal to noise, made toward many more lines of sight, and extended to higher redshifts. The results in the near future should be a definitive detection of the different stages of the reionization era, and the accumulation of a large body of knowledge on the properties of ionizing sources and of the IGM during reionization.

I thank Zoltan Haiman for useful discussions which motivated this work, and George Djorgovski for helpful details regarding his observations. I thank CITA for providing research support and a stimulating research environment.

REFERENCES

- Abel, T., & Mo, H. J. 1998, *ApJL*, 494, 151
- Barkana, R., & Loeb, A. 1999, *ApJ*, 523, 54
- Barkana, R., & Loeb, A. 2001, *Phys. Rep.*, 349, 125
- Becker, R. H., Fan, X., White, R. L., Strauss, M. A., & Narayanan, V. K. 2001, *AJ*, submitted (astro-ph/0108097)

- Bond, J. R., Szalay, A. S., & Silk, J. 1988, *ApJ*, 324, 627
- Cen, R. 2001, *ApJ*, in press (astro-ph/0101197)
- Chiu, W. A., & Ostriker, J. P. 2000, *ApJ*, 534, 507
- Djorgovski, S. G., Castro, S. M., Stern, D., & Mahabal A. 2001, *ApJL*, submitted (astro-ph/0108069)
- Fan, X., et al. 2000, *AJ*, 120, 1167
- Gnedin, N. Y. 2000, *ApJ*, 535, 530
- Gnedin, N. Y., & Ostriker, J. P. 1997, *ApJ*, 486, 581
- Gunn, J. E., & Peterson, B. A. 1965, *ApJ*, 142, 1633
- Haiman, Z., Abel, T., & Rees, M. J. 2000, *ApJ*, 534, 11
- Haiman, Z., & Loeb, A. 1997, *ApJ*, 483, 21
- Haiman, Z., & Loeb, A. 1998, *ApJ*, 503, 505
- Haiman, Z., Rees, M. J., & Loeb, A. 1997, *ApJ*, 476, 458; erratum – 1997, *ApJ*, 484, 985
- Halverson, N. W., Leitch, E. M., Pryke, C., Kovac, J., et al. 2001, *ApJ*, submitted (astro-ph/0104489)
- Kitayama, T., & Ikeuchi, S. 2000, *ApJ*, 529, 615
- Lacey, C. G., & Cole, S. M. 1993, *MNRAS*, 262, 627
- Lee, A. T., Ade, P., Balbi, A., Bock, J., et al. 2001, submitted (astro-ph/0104459)
- Loeb, A., & Barkana, R. 2001, *Annu. Rev. Astron. Astrophys.*, 39, 19
- Magorrian, J., et al. 1998, *AJ*, 115, 2285
- Miralda-Escudé, J. 1998, *ApJ*, 501, 15
- Miralda-Escudé, J., Haehnelt, M., & Rees, M. J. 2000, *ApJ*, 530, 1
- Navarro, J. F., & Steinmetz, M. 1997, *ApJ*, 478, 13
- Netterfield, C. B., Ade, P. A. R., Bock, J. J., Bond, J. R., et al. 2001, *ApJ*, submitted (astro-ph/0104460)
- Quinn, T., Katz, N., & Efstathiou, G. 1996, *MNRAS* 278, L49
- Scalo, J. 1998, in ASP conference series Vol 142, *The Stellar Initial Mass Function*, eds. G. Gilmore & D. Howell, p. 201 (San Francisco: ASP)
- Thoul, A. A., & Weinberg, D. H. 1996, *ApJ*, 465, 608
- Weinberg, D. H., Hernquist, L., & Katz, N. 1997, *ApJ*, 477, 8
- Wood, K., & Loeb, A. 2000, *ApJ*, 545, 86